Chapter 6 Delamination Analysis of Composite Laminates

6.1 Introduction

Composite stiffened panels are being predominantly used as aerospace structures due to their outstanding weight/ stiffness and strength ratio and also ease of repair and assembly under in-situ loading conditions. However, these composite structures are susceptible to interfacial or interlaminar damage mechanisms such as delamination, debonding or such other involvement like matrix crack and fiber breakage due to defects or flaws arising even during manufacturing stages, service or maintenance induced damages, or from low-velocity impact damage or from operational malfunctioning. Many authors have investigated the debonding mechanism and damage propagation of skin/stiffener panels and failure analysis using shell models [55-57] without consideration of manufacturing stage stresses such as thermal residual stresses. These stresses arise when differently oriented stiffeners are assembled and cured from an elevated temperature to room temperature.

This chapter presents the thermo-elastic effect of material anisotropy and residual thermal stresses on interlaminar delamination fracture characteristics of composite stiffened panels. Full three-dimensional coupled field thermo-elastic finite element analyses have been conducted for the preexisting interlaminar delaminations subjected to three-point bending and uniaxial loading. Modified crack closure integral method based on the concept of linear elastic fracture mechanics has been followed to access the individual modes of strain energy release rate along the delamination front. Qualitative comparison has been demonstrated for the individual modes of energy release rate along the delamination front of stiffened panels for both the loadings. The influence of coupled field thermo-elastic

material anisotropy of the constituting laminae has been reasoned for the asymmetric variation of total strain energy release rate along delamination front. This is found to be significantly higher for the case of residual thermal stresses compared to mechanical loading.

6.2 Finite element modeling

A skin-stiffener debonded specimen with lay-up sequence has been considered for analysis. The specimen consists of a bonded skin and flange assembly as illustrated in Figure 6.1. A graphite/epoxy system has been used for both skin and flange. The skin is made up of prepreg tape with a measured average ply thickness of $h_1 = 0.148\,\text{mm}$ and has a [45/-45/0/-45/45/90]$_s$ lay-up. The flange is made up of plain-weave fabric with a thickness of $h_2 = 0.212$ mm. The flange lay-up is $\left[\left(45/0/45/0\right)_2/\overline{45}\right]_{sf}$, where the "$f$" denotes fabric, "0" represents a $0^o - 90^o$ fabric ply and "45" represents a $0^o - 90^o$ fabric ply rotated by 45^o. Specimen is 25.4 mm wide and 101.6 mm long. Adhesive has been applied as an interface element between skin and flange.

Layered 3D solid elements have been used in the present study to model the whole analysis domain and the delamination characteristics are simulated by using multi-point constraints along the delaminated interface. The interface resin layer, in which the delamination is pre-existing, has the properties of a low modulus isotropic material. Adhesive has been used as the interface layer between skin and flange. The interlayer is modeled as two separate layers, having identical isotropic properties, located above and below the delamination plane. The fiber angles are measured counter-clockwise from the x-axis. Inside the delamination zone compatible contact/gap elements are used to prevent the interpenetration

of top and bottom layer, which otherwise would make the analysis physically unrealistic. Progressive propagation of delamination front has been realized by judiciously removing the constraints along the interface of adjacent sublaminates.

The skin/stringer specimen is subjected to tension and three-point bending load. First set of finite element interlaminar fracture analysis is executed for a purely mechanical loading in the form of tensile and bending loads (as shown in Figure 6.2). The second set is thermo elastic fracture behavior in which mechanical loading is applied subsequent to the uniform temperature drop from stress free state at 160^{o} C to 30^{o} C room temperature to induce thermal residual stresses in the laminate. In the third set of analysis, only thermal residual stresses have been applied through uniform temperature drop.

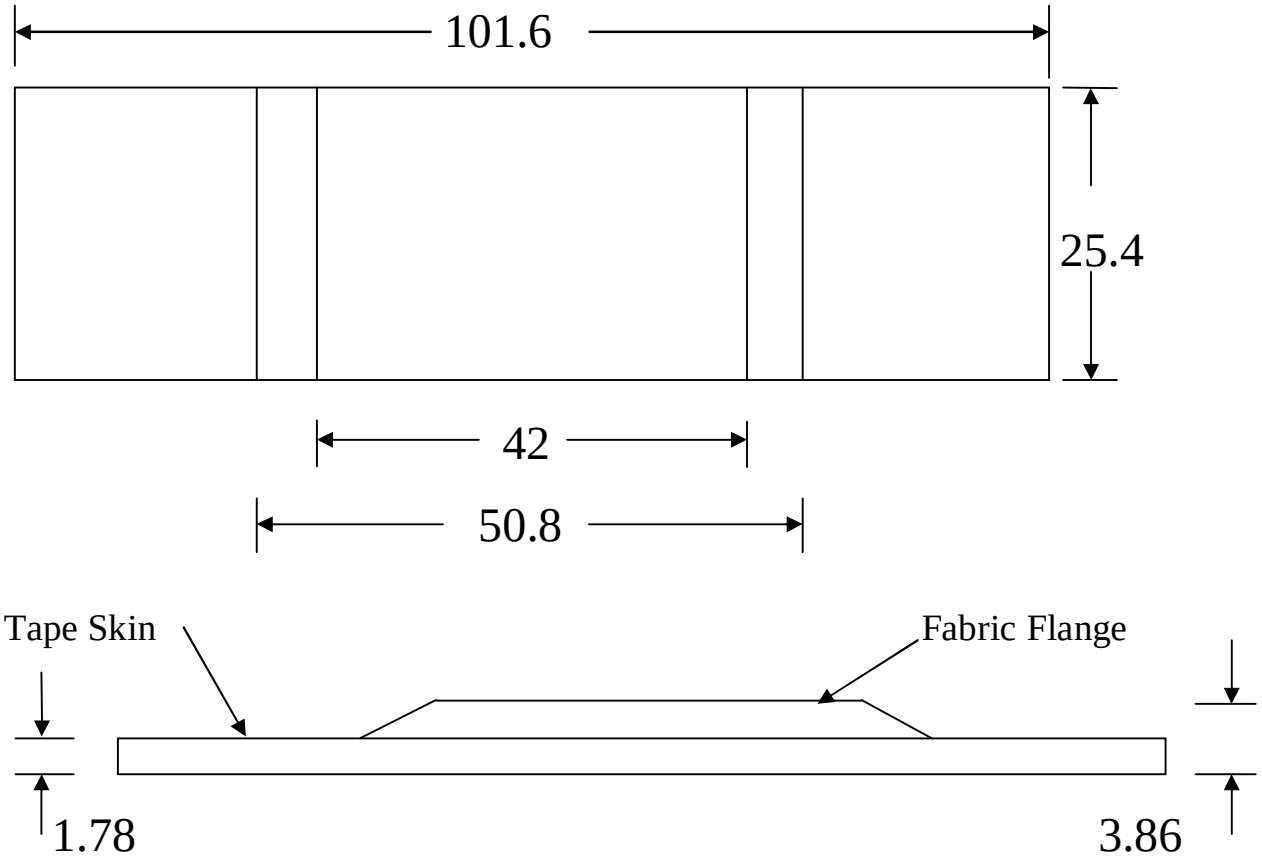

Figure 6.1 Specimen configuration (dimensions in mm.)

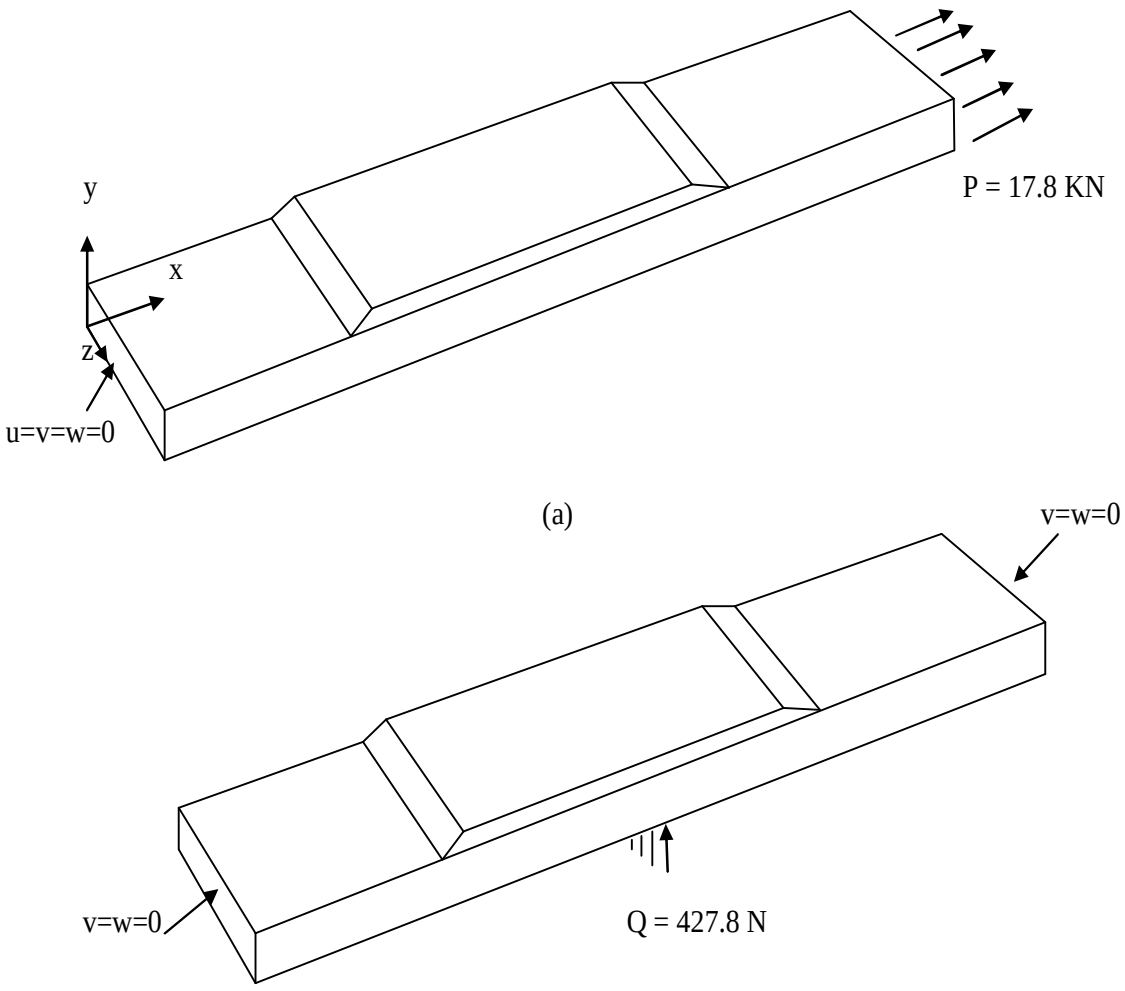

Figure 6.2 3D model of (a) Tensile and (b) bending specimen with load

The stress state has been evaluated throughout the composite laminate using finite element analysis software ANSYS 14.5. Eight-node layered brick element (Solid 185) with three degrees of freedom (translations in the X, Y and Z directions) at each node has been used to model the analysis domain. The orthotropic thermo-elastic material properties of the graphite/epoxy material and the adhesive are summarized in Table 6.1.

Table 6.1 Thermoelastic material properties [180,181]

	Unidirectional prepreg	Plain-weave fabric	Adhesive
Elastic Properties			
E_{11} (GPa) E_{22} (GPa) E_{33} (GPa)	161.0 11.38 11.38	71.7 71.7 10.3	E = 1.72 (GPa)
G_{12} (GPa)	5.17	4.48	G = 1.42 (GPa)
G_{13} (GPa)	5.17	4.14	
G_{23} (GPa)	3.92	4.14	
ν_{12}	0.32	0.04	ν = 0.3
ν_{13}	0.32	0.35	
ν_{23}	0.45	0.35	
Thermal Properties			
$\alpha_x (/^oC)$	0.025 X 10^{-6}	0.02 X 10^{-6}	α = 44 X 10^{-6} (/°C)
$\alpha_y (/^oC)$	0.025 X 10^{-6}	0.02 X 10^{-6}	
$\alpha_z (/^oC)$	22.5 X 10^{-6}	19.5 X 10^{-6}	
Temperature state: Curing temperature = 160 °C Room temperature = 30 °C ΔT = -130 °C			

Boundary conditions

(a) For tensile loading, the displacement boundary conditions imposed are

For all nodes at $x = 0, u = v = 0$ for $0 \le z \le 25.4$ mm

$$w = 0 \text{ for } z = 12.7 \text{ mm}$$

along $z - axis$, $v = 0$ at $x \ge 101.6$ mm

(b) For bending, boundary conditions are

For all nodes at $x = 0, v = 0$ for $0 \le z \le 25.4$ mm

$$u = w = 0 \text{ for } z = 12.7 \text{ mm}$$

For all nodes at $x = 101.6mm, v = 0$ for $0 \le z \le 25.4$ mm

$$w = 0 \text{ at } z = 12.7 \text{ mm}$$

where u, v and w are the displacements along the X, Y and Z directions, respectively.

Under the application of loading and boundary conditions, the flange gets debonded from the skin. The location and the damage pattern of the debonding have been shown in Figures 6.3 and 6.4, respectively. Figure 6.5 shows the meshing pattern of the laminated specimen. In three dimensional finite element analysis, the mesh has been made progressively finer as it approaches the delamination front along the interface. Relevant error analyses and mesh refinements have been carried out for convergence. Figure 6.6 shows the zoomed view of finite element (FE) model developed for studying the thermo-elastic effect on fracture crack growth behavior of embedded interface delamination for the multilayered graphite/epoxy laminate specimen. It can be illustrated from figure that refined mesh has been done at the critical area where the crack is observed during the test. The displacements and stresses are obtained from three dimensional finite element analysis. Under the reasonable temperature variation from curing state to room temperature both thermo-physical and mechanical properties are assumed to remain unchanged.

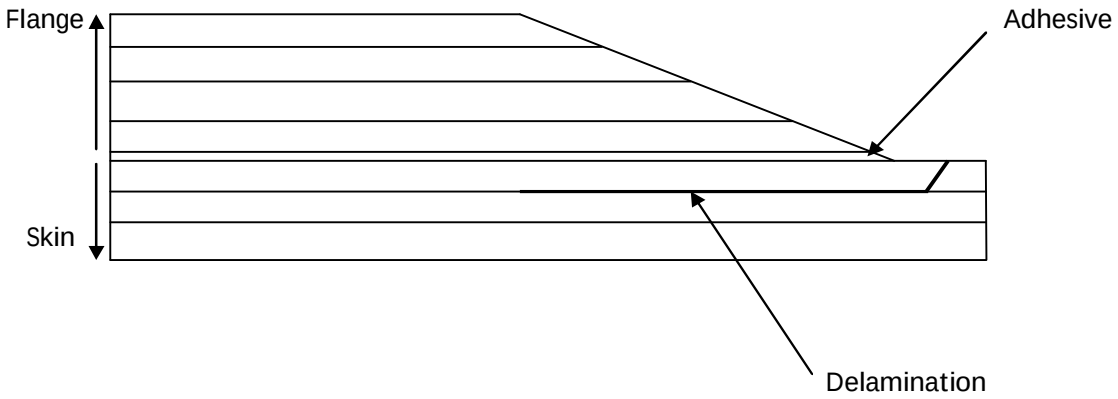

Figure 6.3 Location of delamination in specimen

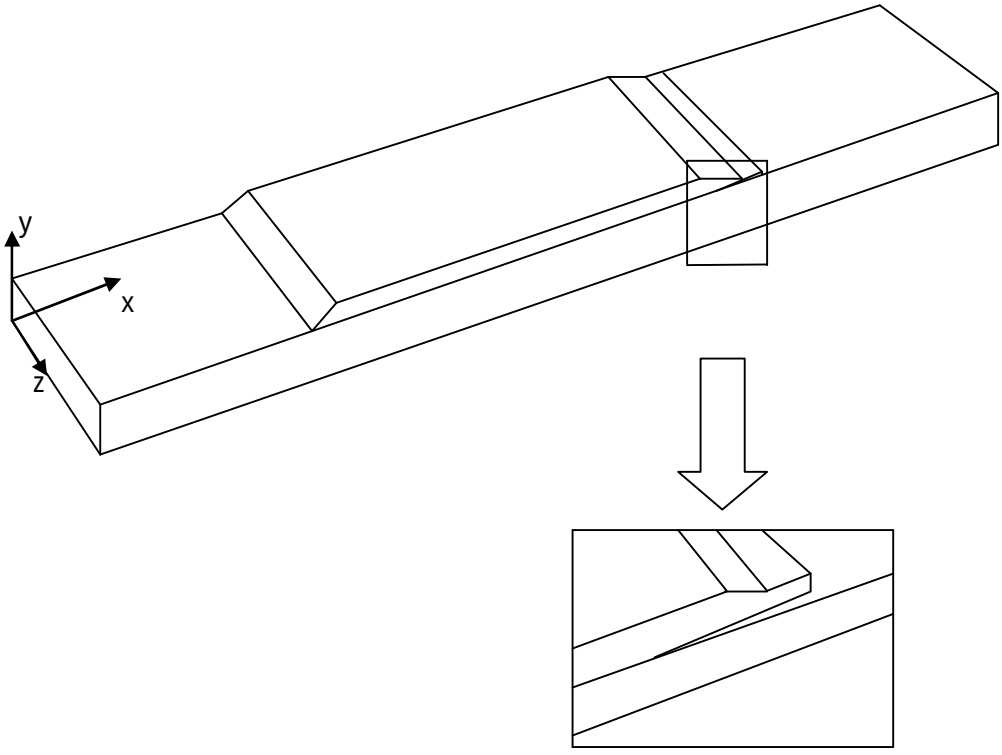

Figure 6.4 Typical damage pattern observed in skin-stiffener specimen

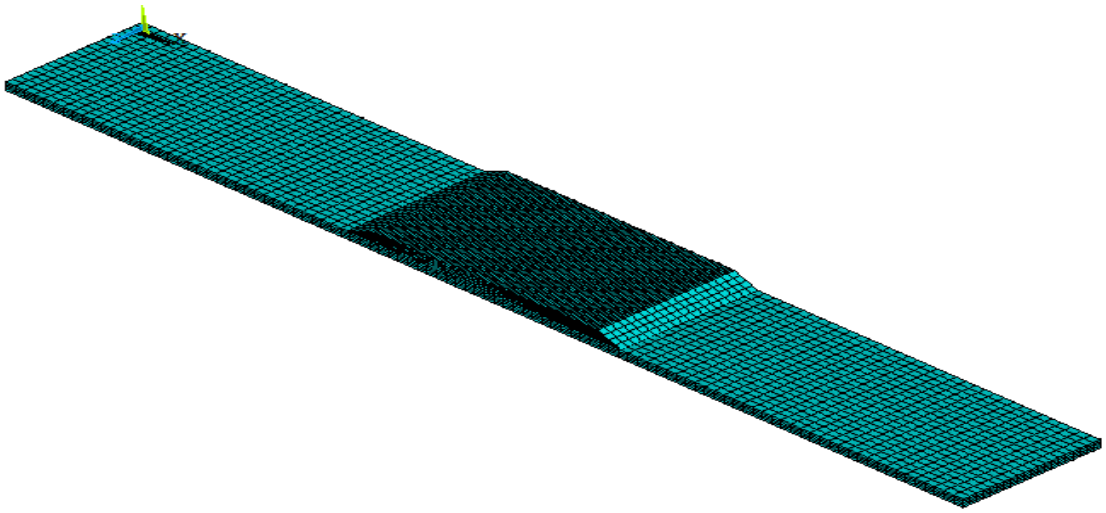

Figure 6.5 Finite element modeling of the graphite/epoxy specimen with embedded delamination at the interface

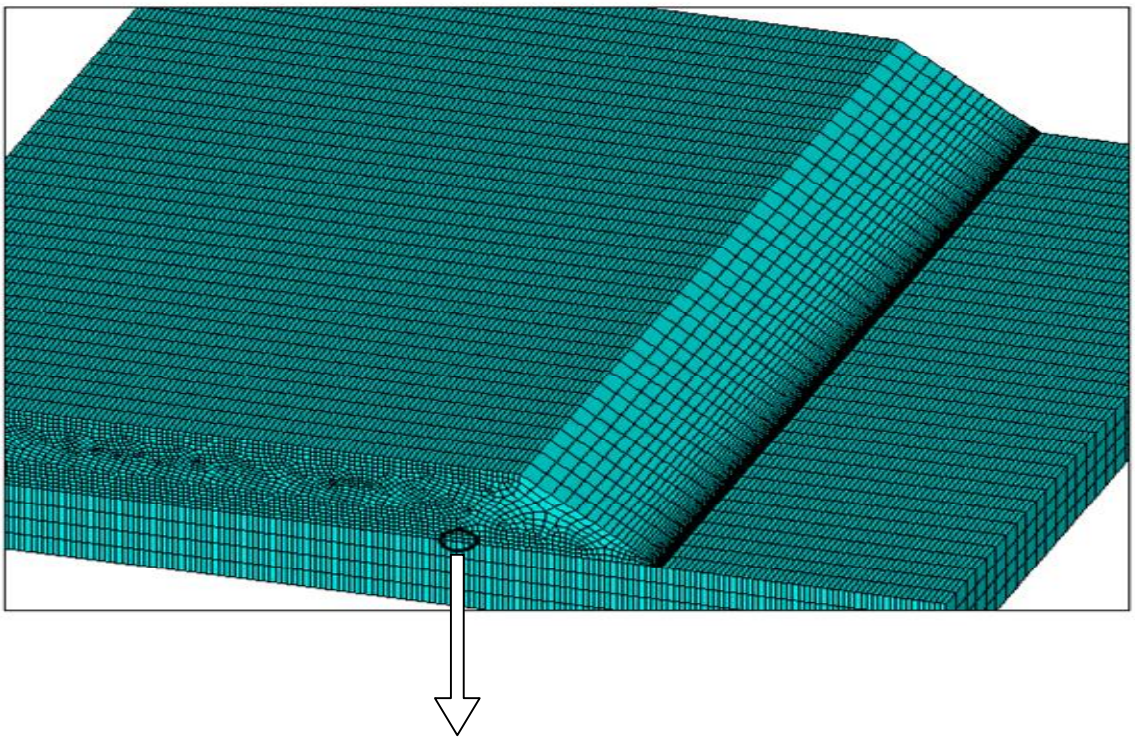

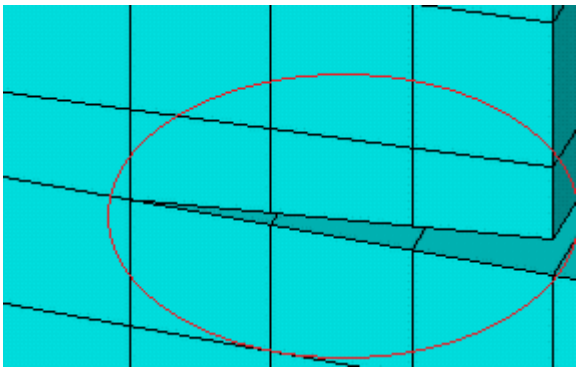

Figure 6.6 Zoomed view of FE model for stiffened panel

6.3 Results and discussion

In steady-state non-linear finite element analyses, strain energy release rates are generally computed at each front location for the loads applied. While in the present analysis, the results are computed across the width of the specimen, i.e., at $x = 62.23mm$. Full 3D thermo-elastic finite element analyses have been carried out to account the possibility of bending-stretching coupling due to thermo-mechanical loading on laminated specimen for bending and tensile loading. Mode I, Mode II and Mode III strain energy release rates primarily spread over a subsequential zone of delamination front. The asymmetric distributions are found to be different for different types of loading. Also, the total energy release rate $G_T = G_I + G_{II} + G_{III}$, along the centerline of the specimen is obtained from 3D analysis. Distribution of individual modes of strain energy release rate along the delamination front for different loading condition on laminated composite have been discussed below.

6.3.1 Three-point bending load

Figures 6.7-6.10 illustrate the delamination crack growth behavior of various parameters of strain energy release rate distribution. The delamination crack growth studies have been accomplished and strain energy release rate along delamination front are evaluated from

stresses and displacement obtained from three dimensional thermo-elastic analysis. The distribution is non-uniform along the length, i.e., from $z = 0$ to $25.4mm$. The comparison is done between the values of $G_I, G_{II}, G_{III}, G_T$ and width of specimen when skin stiffener is subjected to mechanical and thermo-mechanical loading under three-point bending. Table 6.2 shows the various values of SERR evaluated for different modes under thermo-mechanical loading. Figure 6.7 shows the variation of G_I for different values of width of the specimen. It has been observed that ERR value for two different loadings are different. Value of G_I is dominant for thermo-mechanical except some places where it is higher for mechanical loading.

Figure 6.8 demonstrates that ERR value for both types of loading is approximately same. The similarity in the energy release rate value is due to the less effect of thermal residual stress on interlaminar sliding shear. Referring to the mode III, there is large variation in the values of energy for both stresses (Figure 6.9). There is very less variation in the value of G_{III} in case of thermo-mechanical loading. Referring to the mechanical loading, the energy release rate attains very high value and the maximum is 1.025 J/m^2. According to Figure 6.10, there is a mismatch in EER for both mechanical and thermo-mechanical along the delamination front. The domination of fracture rate in case of thermo-mechanical is due to the thermal residual stresses. Referring to the Figure 6.11, the fracture energy associated with total mode interlaminar delamination crack propagation shows characteristically different patterns of energy release rate distribution for mechanical, thermal and thermo-mechanical loadings. The asymmetry in the values of G_T is higher for the thermo-mechanical coupled field comparing to mechanical and thermal loading applied alone. For all loadings, the initial energy value is low and then it increases. The maximum G_T occurs

at $z = 25\text{mm}$ for thermo-mechanical loading. More over along the width, the fracture energy possesses lower value for thermal in comparison to thermo-mechanical and mechanical loading.

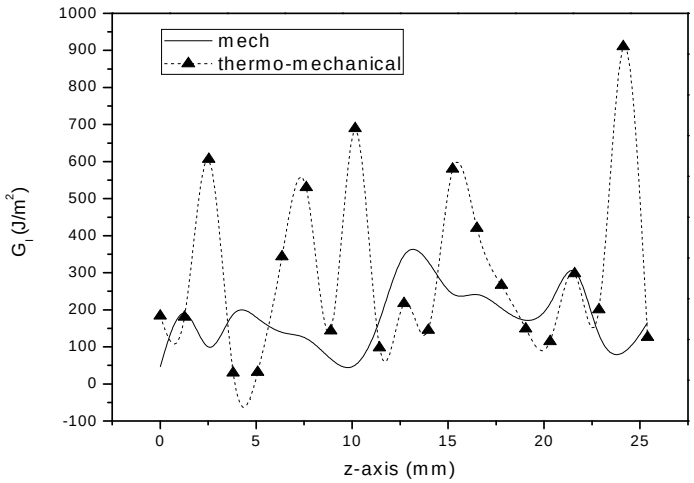

Figure 6.7 Comparison of G_I distribution at different width along delamination front for three point bending

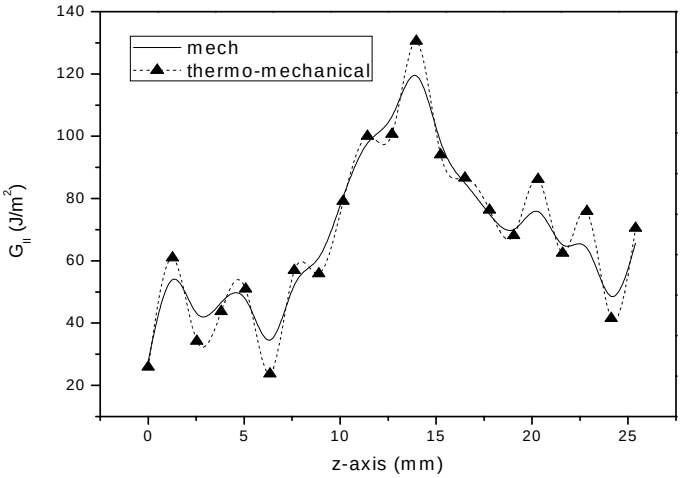

Figure 6.8 Comparison of G_{II} distribution at different width along delamination front for three point bending

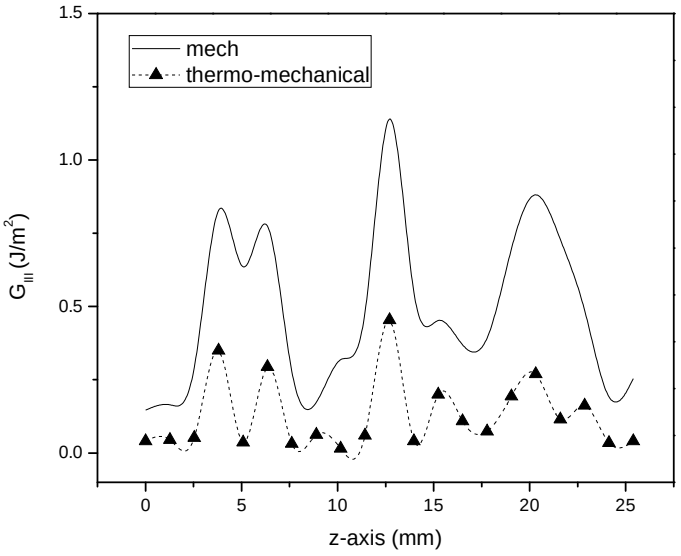

Figure 6.9 Comparison of G_{III} distribution at different width along delamination front for three point bending

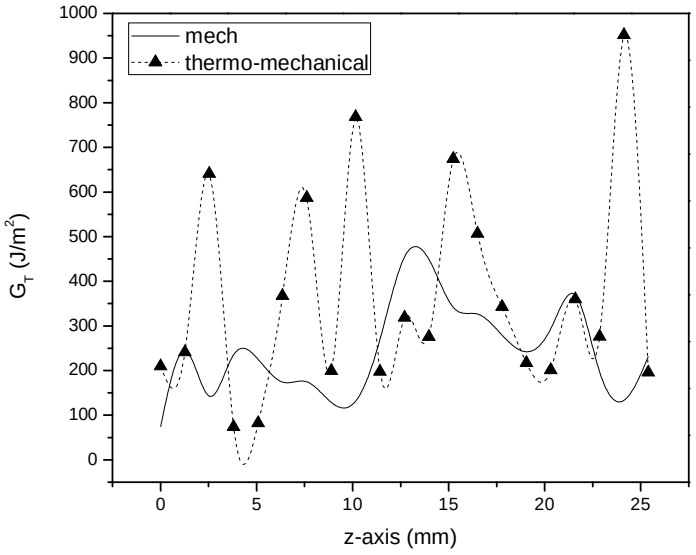

Figure 6.10 Comparison of G_T distribution at different width along delamination front for three point bending

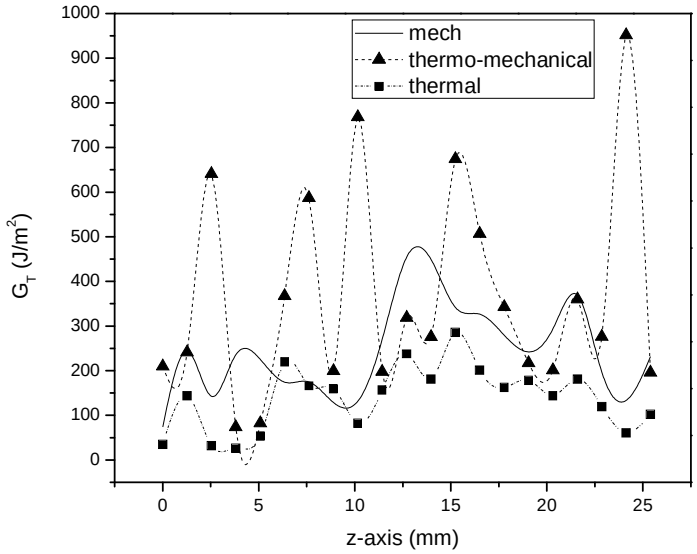

Figure 6.11 Comparison of G_T distribution at different width along delamination front for three point bending under various loadings

Table 6.2 Strain energy release rates for the delamination under thermo-mechanical loading for three point bending

Node No.	G_I	G_{II}	G_{III}	G_T
141	183.78	25.897	0.04048	209.72
3671	180.3	60.945	0.04522	241.29
3672	606.54	34.196	0.05183	640.78
3673	29.691	43.725	0.34997	73.766
3674	31.676	50.952	0.03639	82.75
3675	343.54	23.686	0.29401	367.52
3676	530.33	56.948	0.03187	587.31
3677	143.61	55.888	0.06238	199.56
3678	689.26	79.156	0.01555	768.43
3679	97.58	100.02	0.06001	197.66
3680	217.46	100.66	0.45372	318.58
3681	145.39	130.53	0.04045	275.96
3682	579.83	94.064	0.19982	674.09
3683	420.12	86.581	0.10843	506.81
3684	266.67	76.332	0.07377	343.08
3685	149.01	68.115	0.19388	217.32
3686	114.58	86.205	0.26988	201.05
3687	297.57	62.476	0.11531	360.16
3688	200.51	75.889	0.16225	276.56
3689	910.43	41.542	0.03492	952.01
646	125.6	70.497	0.0408	196.14

6.3.2 Tensile Load

Figures 6.12-6.15 show the deviation of energy release rate w.r.t width around the delamination front for epoxy laminate under tensile loading. The analysis has been carried out for uniform temperature drop and subsequent tensile loading upon the prestresses laminate. Strain energy release rates have been calculated for the modes G_I , G_{II} , G_{III} and G_T under thermo-mechanical loading are mentioned in Table 6.3. Similar to the bending load, here also ERR fluctuates rapidly for mechanical and thermo-mechanical loading. Mode I interlaminar fracture energy release rate as a parameter of distribution with respect to various width position over the delamination zone has been displayed in Figure 6.12. Maximum energy value is 450 J/m^2 at z = 14mm along delamination front for the thermo-mechanical loading indicating the severity of delamination propagation at this point. Similar to the bending, G_{II} has nearly same value for both mechanical and thermo-mechanical (Figure 6.13). Maximum G_{II} occurs at the middle part of width and then gradually decreases.

The variations of mode III and total ERR with respect to z -axis have been described in Figures 6.14 and 6.15, respectively, considering the thermal residual stresses and mechanical loading. From the figures, it is revealed that initial values of G_{III} is approximately same for both loadings. The significant difference between G_{III} values along the delamination front recommends the criticality of effect of interlaminar residual stresses developed due to initial thermal loading on laminated specimen. Near the edges of specimen, energy release rate attains lowest value for mechanical load and at the center it has higher value. Similar difference has been observed for thermo-mechanical, but the energy value is higher compared to former. Figure 6.15 shows the variation and dominance

of the total ERR under the coupled effect of thermal and mechanical loading along the delamination front. The interval from 0 to 25.4mm width position of delamination front, there is a marked difference in energy due to thermal residual stresses. The energy has its highest value at z =14mm.

Figure 6.16 depicts the variation of total rate along the delamination front for mechanical, thermal and thermo-mechanical loadings. Transition of thermo-elastic stress field along the delamination front causes SERR values unevenly distributed around it. For all three types of loading, maximum energy is at the center of the width of the specimen. It is also illustrated from figure that the nature of graph for thermo-mechanical and thermal is nearly same. The multiple peaks in ERR plots at various locations unlike a monolithic cracked structural component.

It can be noted from energy release rate analysis of tensile and three point bend loads that the coupling effect of thermal residual stresses in some cases, magnifies the mixed-mode interlaminar delamination crack growth, whereas in others, it also disagrees the interface crack growth mechanism depending upon the location of embedded delamination front. The variation of SERR explains the physical mechanism behind the constrained delamination propagation in composite laminates. The effects become more affirmed at most of the peaks, either decreasing the energy release rate values or by intensifying it for individual modes.

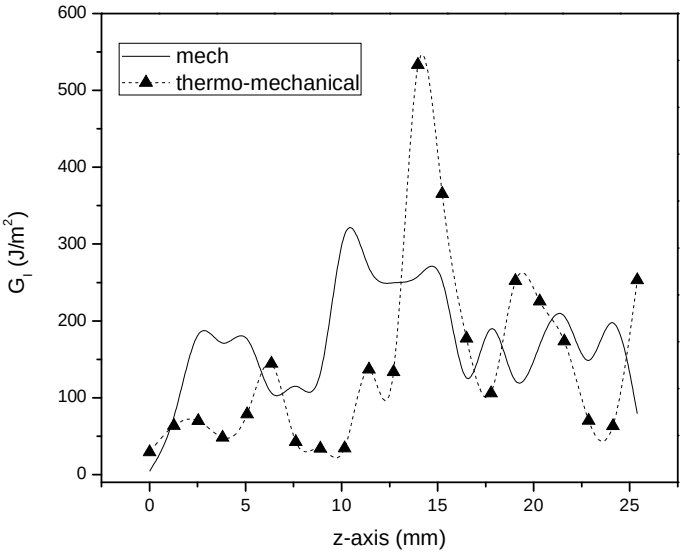

Figure 6.12 Comparison of G_I distribution at different width along delamination front for tension

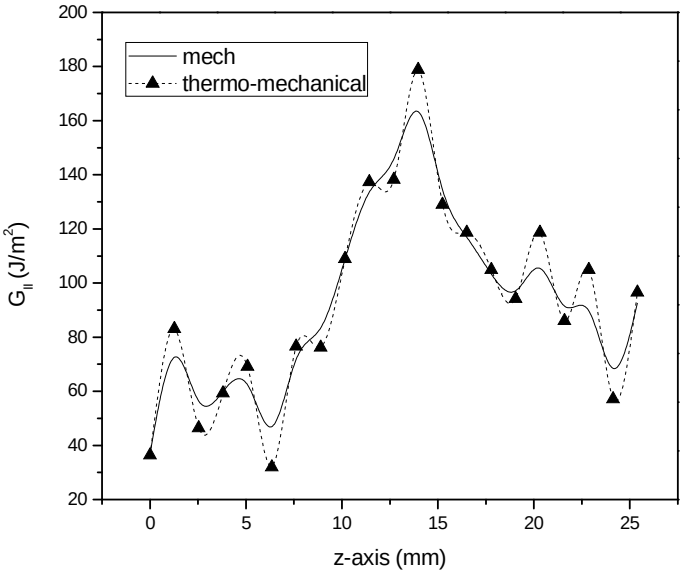

Figure 6.13 Comparison of G_{II} distribution at different width along delamination front for tension

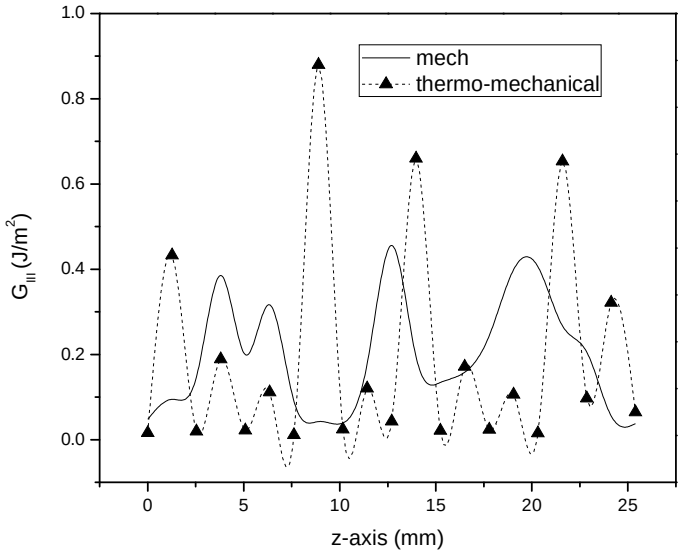

Figure 6.14 Comparison of G_{III} distribution at different width along delamination front for tension

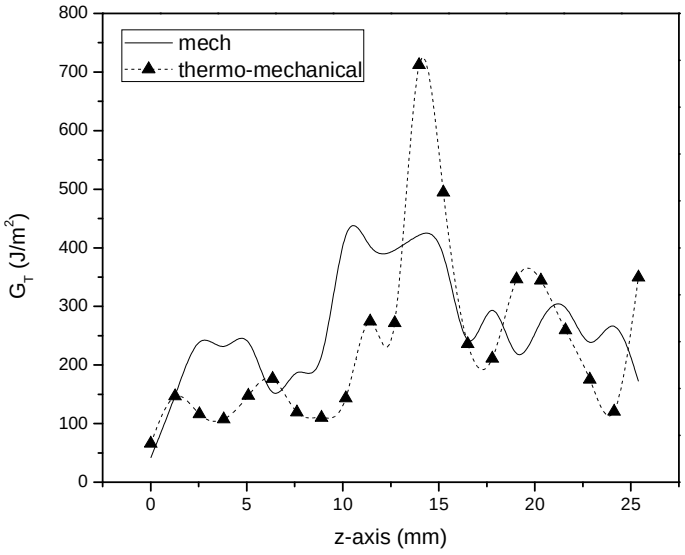

Figure 6.15 Comparison of G_T distribution at different width along delamination front for tension

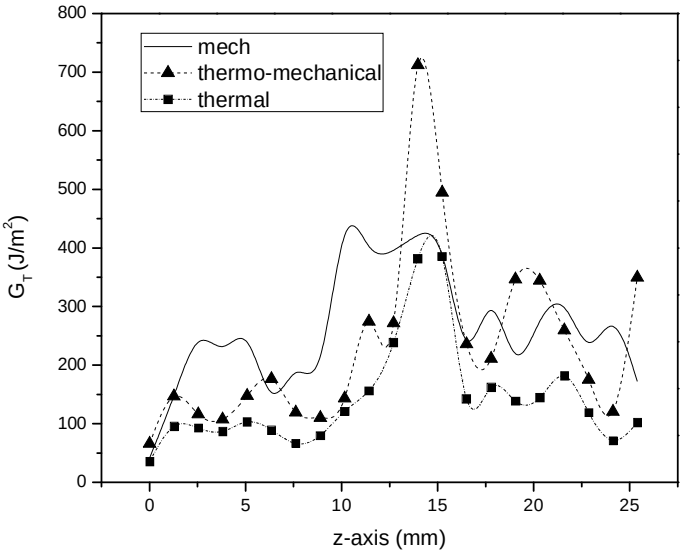

Figure 6.16 Comparison of G_T distribution at different width along delamination front for tension under various loading

Table 6.3 Strain energy release rates for the delamination under thermo-mechanical loading for tension

Node No.	G_I	G_{II}	G_{III}	G_T
141	29.376	36.401	0.01598	65.779
3671	63.782	83.084	0.4327	146.87
3672	69.867	46.454	0.01955	116.32
3673	48.232	59.288	0.1889	107.54
3674	78.558	69.136	0.02174	147.7
3675	144.59	31.98	0.11155	176.58
3676	42.493	76.578	0.01107	119.07
3677	34.005	76.227	0.88	110.23
3678	34.451	108.96	0.0244	143.41
3679	136.87	137.34	0.1203	274.2
3680	133.63	138.24	0.0432	271.87
3681	533.37	178.82	0.66	712.19
3682	365.53	129.03	0.02116	494.56
3683	177.36	118.72	0.1714	236.09
3684	106.08	104.92	0.02356	211
3685	252.12	94.195	0.1061	346.33
3686	225.63	118.71	0.01514	344.35
3687	173.4	86.03	0.65333	259.44
3688	70.195	104.9	0.09722	175.11
3689	63.233	57.142	0.3215	120.38
646	253.03	96.552	0.0644	349.59

6.4 Conclusion

In the three-dimensional thermo-elastic analysis, modeling and simulation of interlaminar delaminations have been conducted for FRP composite laminates subjected to bending and tensile loading. Effects of material properties and thermal residual stresses on progressive delamination front propagation have been studied. Strain energy release rate procedure has been adopted to study the thermo-elastic fracture behavior of the embedded interlaminar delamination. It is to be noted that due to the constraining effect of the thermal residual stresses and the interaction of the thermo-elastic stress field, energy release rate plots exhibit unsymmetrical variation with respect to the width of the specimen along the delamination front. Following conclusions are drawn from the investigation of delamination behavior in the composite material due to residual stresses.

1. In a multi-lay up laminate, the thermo-elastic properties put a restrainting effect on the adjacent plies at the interface. The residual thermal stresses evolved may retard or magnify the mechanism of delamination growth depending upon the loading type.

2. The asymmetries in strain energy rate plots obtained with and without considering the thermo-elastic superposed effect of residual stresses is due to the anisotropy ratio of thermal expansion.

3. First mode of energy release rate is the most dominant component of the total energy release rate and plays a salient role in characterizing the delamination crack growth behavior and failure of composite laminates for both three point bending and tensile loading.

This work signifies the relative influence of residual thermal stresses and loading condition on the delamination propagation behavior in FRP laminates and consequently should be taken into account in damage development studies.

This chapter includes the effect of curing stress on skin-stiffener. Moreover, effect of bimodularity along with curing stress and different loading conditions should be study for development of high efficient and durable composites. This has been complied in next chapter.